PCCP

Accepted Manuscript

ROYAL SOCIETY OF CHEMISTRY

www.rsc.org/pccp

Physical Chemistry Chemical Physics
CREATED USING THE RSC LaTeX PCCP ARTICLE TEMPLATE – SEE www.rsc.org/electronicfiles FOR DETAILS
ARTICLE TYPE www. rsc.org/xxxxxx | XXXXXXXX

Boron nitride zigzag nanoribbons: optimal thermoelectric systems

K. Zberecki[1], R. Swirkowicz[1], J. Barnaś[2]

Received Xth XXXXXXXXXX 20XX, Accepted Xth XXXXXXXXX 20XX
First published on the web Xth XXXXXXXXXX 200X
DOI: 10.1039/b000000x

Conventional and spin related thermoelectric effects in zigzag boron nitride nanoribbons are studied theoretically within the Density Functional Theory (DFT) approach. Nanoribbons with edges passivated with hydrogen, as well as those with bare edges are analyzed. It is shown, that one spin channel in the nanoribbons of 0HB-0HN and 2HB-1HN types becomes nonconductive slightly above the Fermi level, and therefore such nanoribbons reveal remarkable spin related thermoelectric phenomena and are promising materials for thermoelectric nanodevices. Thermoelectricity in BN nanoribbons of other types is less efficient and therefore these materials are less interesting for applications.

1 Introduction

Since the two-dimensional (2D) boron nitride (BN) was synthesized, one can observe an increasing interest in this novel low-dimensional material.[1–10] Similarly to graphene, silicene, or stanene, boron nitride is a 2D crystal of hexagonal atomic structure. Its electronic properties, however, are essentially different, as it is an insulator with a wide energy gap.[11,12] Interestingly, this material exhibits high chemical stability, which is a very important feature from the point of view of potential applications.[13] Boron nitride nanoribbons (BNNRs) also turned out to be stable and – similarly to graphene nanoribbons (GNRs) – they can be obtained by cutting BN sheets or by un-zipping BN nanotubes.[14]

Various types of the edge termination in the nanoribbons can be observed, including armchair and zigzag nanoribbons with B-edges (bare or passivated) or N-edges (bare or passivated). Their physical properties are remarkably different from those of GNRs, mainly due to typical ionic nature of the B-N bonds. From theoretical considerations follows that electronic and magnetic properties of zigzag BNNRs (in the following referred to as zBNNRs) are determined by the type of their edges, and also depend on whatever the B or N edges remain bare or they are terminated with hydrogen atoms.[15–17] Generally, zBNNRs with bare B or N edges can be magnetic as the dangling bonds at the edges induce magnetic moments.[18] Ribbons with bare B-edge or B-edge terminated with hydrogen atoms are half-metallic, whereas those with N-edge or both edges being terminated with hydrogen are mainly semiconducting.[19] Interestingly, zBNNRs asymmetrically terminated with fluorine exhibit half-metallic behavior and 100% spin polarization around the Fermi level[20]. Accordingly, different termination of zBNNRs allows controlling their electronic and magnetic properties. It has been also shown that the band gap of zBNNRs can be significantly tuned by a uniaxial tensile strain.[21] Apart from this, a magnetic tunnel junction consisting of BNNRs contacted to two ferromagnetic graphene electrodes was also studied, and such a junction turned out to be a very effective spin filter.[22]

It is known that boron nitride nanostructures exhibit relatively high thermal conductance, which however is considerably lower than the thermal conductance of the carbon-based counter-parts.[23] There are two reasons of such behavior, namely softer phonon modes in systems based on boron nitride, as well as a difference in atomic mass of B and N atoms.[23] Owing to the lower heat conductance, BNNRs seem to be interesting from the point of view of the corresponding thermoelectric properties.

Generally, thermoelectric phenomena in nanostructures are currently of great interest, mainly due to a possibility of heat into electric energy conversion at nanoscale. Many papers have appeared, mainly theoretical, concerning thermoelectric properties of novel nanomaterials, especially graphene and GNRs of various types.[24–31] However, carbon-based nanostructures are not good thermoelectric materials, as the thermoelectric efficiency is rather low due to exceptionally high phonon thermal conductance. Thus, it is very important to search for nonomaterials with optimal thermoelectric properties. To enhance thermoelectric efficiency, hybrid systems based on graphene and BN have been proposed, in which BN is periodically embedded into GNRs.[32] Thermal conductance of such hybrid nanoribbons can be considerably reduced while the Seebeck coefficient can be enhanced.

In this paper we study thermoelectric effects in zBNNRs and demonstrate outstanding properties of nanoribbons with

[1] *Faculty of Physics, Warsaw University of Technology,ul. Koszykowa 75, 00-662 Warsaw, Poland*
[2] *Faculty of Physics, Adam Mickiewicz University, ul.Umultowska 85, 61-614 Poznań, Poland*
and Institute of Molecular Physics,Polish Academy of Sciences, Smoluchowskiego 17, 60-179 Poznań, Poland

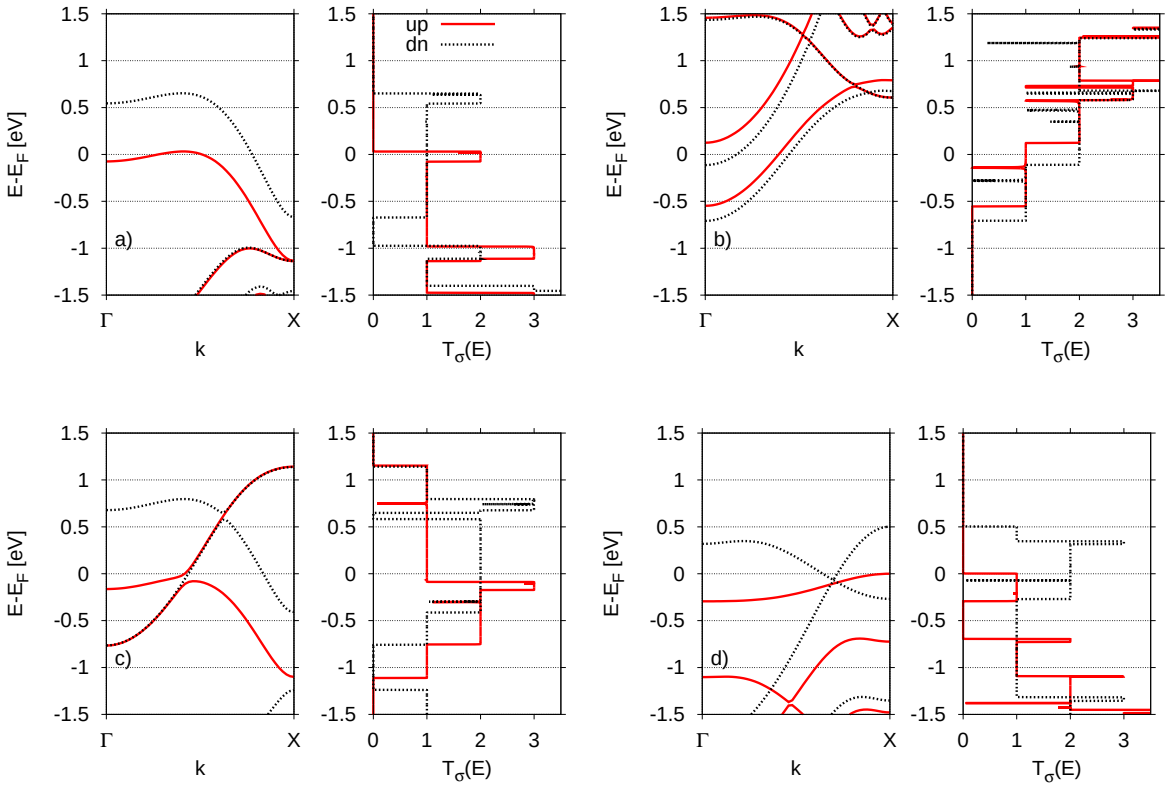

Fig. 1 (Color online) Band structure and spin-resolved transmission function $T_\sigma(E)$ of zBNNRs of the following types: a) 2HB-1HN, b) 1HB-2HN, c) 2HB-2HN, and d) 0HB-0HN. Only a narrow energy region in a close vicinity of the Fermi energy E_F is presented. Here, up and dn stand for the spin-up and spin-down channels, respectively. The nanoribbons consist of $N = 6$ zigzag atomic chains, while the other parameters as described in the text.

some specific edges, which exhibit remarkably enhanced thermoelectric efficiency. Moreover, our calculations also show that zBNNRs with two bare edges as well as those asymmetrically terminated with hydrogen in such a way that the B-edge is di-hydrogenated while the N-one is monohydrogenated, exhibit ferromagnetic ordering. In addition to conventional thermoelectricity, such nanoribbons also reveal spin related thermoelectric phenomena.[33–37] The spin Seebeck effect, which is a spin analog of the conventional Seebeck effect, was observed experimentally in thin films[38] and tunnel junctions.[39,40] While the latter effect describes electrical voltage generated by a temperature gradient, the former effect corresponds to thermally generated spin voltage. The spin Seebeck effect originates from the interplay between charge, spin and heat transport. Our investigations show that the conventional and spin Seebeck effects are remarkably enhanced in the above mentioned zBNNRs due to a specific band structure leading to rapid decrease of transmission near the Fermi level in one spin channel, whereas the second spin channel remains fully conductive. Moreover, thermal conductance due to electrons, κ_e, is reduced in the region of chemical potential corresponding to the main peak in the thermopower S, but the electrical conductance G is still relatively high. It is also important that the thermal conductance due to phonons, κ_{ph}, is much lower in BNNRs in comparison to carbon-based nanostructures.[23] As a result, thermoelectric efficiency described by thermoelectric figure of merit $ZT = GS^2T/(\kappa_e + \kappa_{ph})$, with T denoting the temperature, is remarkably enhanced. Accordingly, the nanoribbons under consideration appear to be optimal thermoelectric materials, with a great potential for applications in nanoelectronics and spintronic devices.

2 Computational details

Electronic band structure of zBNNRs containing N zigzag atomic chains was determined within the Density Functional Theory (DFT) using the Generalized Gradient Approximation

(GGA).[41,42] The structures were optimized until atomic forces converged to 0.02 eV/Å. Furthermore, we used the atomic double-polarized basis (DZP), while the grid mesh cutoff was set equal to 200 Ry. In turn, for calculating the spin-resolved transmission function we have employed the Non-equilibrium Green Function (NGF) method, as implemented in the Transiesta code.[43,44]

To study the influence of hydrogen termination of zBNNRs on their electronic, magnetic and transport properties, we have performed systematic calculations for various types of nanoribbons, i.e. for nanoribbons with bare edges as well as for those terminated with one or two hydrogen atoms. We have considered the situations when the hydrogen atoms are attached symmetrically or asymmetrically to both edges. For convenience, we will use the following notation: (i) 2HB-1HN for the nanoribbon in which the B-edge is di-hydrogenated, while the N-edge is mono-hydrogenated, (ii) 1HB-2HN for nanoribbons with the B-edge and N-edge being mono- and di-hydrogenated, respectively, and (iii) 2HB-2HN for nanoribbons with both edges terminated with two H atoms. Additionally, we also present results for the nanoribons of 0HB-0HN type, with both bare edges. The obtained numerical results show that the most stable systems are the zBNNRs of 2HB-1HN type, whereas the corresponding nanoribbons of 0HB-0HN type have the highest energy.

3 Electronic structure and transmission function of zBNNRs

The calculated electronic band structures, shown in Fig. 1, clearly show that the zBNNRs under consideration exhibit metallic transport features (nonzero electron density at the Fermi level E_F of the corresponding charge-neutral nanoribbon). Additionally, in Fig. 1 we also present the spin-resolved transmission function, $T_\sigma(E)$. As one can see, the hydrogen atoms at the nanoribbon's edges strongly influence its electronic band structure and also the corresponding transmission function. In a close vicinity of the Fermi level E_F, the transmission function in the case of 2HB-2HN and 1HB-2HN zBNNRs is high and constant in both spin channels, which indicates that these systems can not exhibit remarkable thermoelectric properties. Qualitatively different behavior can be expected in the case of 0HB-0HN and 2HB-1HN nanoribbons. In both these systems, one spin channel becomes nonconductive just above the Fermi level E_F, which can strongly influence their thermoelectric properties. First, this leads to an enhanced Seebeck coefficient. Second, these nanoribbons exhibit ferromagnetic ordering of the edge magnetic moments, so the spin related thermoelectric effects can also be revealed. Therefore, in the following we will focus mainly on these zBNNRs.

4 Thermoelectric properties of 2HB-1HN zBNNRs

Nanoribbons of 2HB-1HN type exhibit ferromagnetic ordering, i.e. magnetic moments localized at the B dihydrogenized edge are parallel, while the moments at the other edge are vanishingly small. Spin density calculated for such a nanoribbon is presented in Fig. 2, where the magnetic moment per unit cell is equal to 5.53 μB.

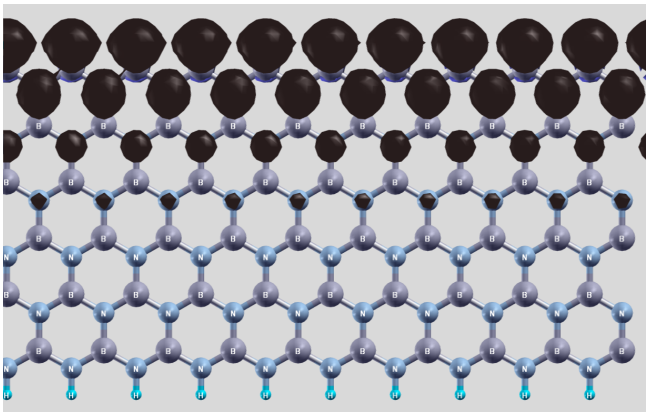

Fig. 2 (Color online) Spin density distribution for the zBNNR of 2HB-1HN type with $N = 6$ zigzag atomic chains. Such a nanoribbon exhibits ferromagnetic alignment of the edge moments. These moments are localized at the B dihydrogenized edge.

In ferromagnetic systems, in which the two spin channels can be treated as independent and do not mix on the nanoribbon length, the spin effects become important and may be revealed in thermoelectric properties. In the presence of a temperature gradient ΔT, a spin voltage ΔV_s can be then generated in addition to the conventional electrical (or charge) voltage ΔV, which give rise to the spin Seebeck coefficient $S_s = -\Delta V_s/\Delta T$ as well as to the conventional Seebeck coefficient $S_c = -\Delta V/\Delta T$. Assuming that both S_c and S_s are determined under the condition of zero charge I and spin I_s currents, the Seebeck coefficients in the linear response regime can be calculated according to the following formulas:[36]

$$S_c = -\frac{1}{2|e|T}(L_{1\uparrow}/L_{0\uparrow} + L_{1\downarrow}/L_{0\downarrow}),$$
$$S_s = -\frac{1}{2|e|T}(L_{1\uparrow}/L_{0\uparrow} - L_{1\downarrow}/L_{0\downarrow}), \quad (1)$$

where $L_{n\sigma} = -\frac{1}{h}\int dE\, T_\sigma(E)\,(E-\mu)^n \frac{\partial f}{\partial E}$ for n=0,1,2. Here, $T_\sigma(E)$ is the spin-dependent transmission function, $f(E-\mu)$ is the Fermi-Dirac distribution function corresponding to the chemical potential μ and temperature T (equal in both electrodes in the linear response description). The electrical conductance in the spin channel σ is then given by the formula

$G_\sigma = e^2 L_{0\sigma}$, while the thermal conductance κ_e due to electrons is equal to

$$\kappa_e = \frac{1}{T}\sum_\sigma \left(L_{2\sigma} - \frac{L_{1\sigma}^2}{L_{0\sigma}} \right). \quad (2)$$

Thermoelectric coefficients of the 2HB-1HN zBNNRs have been calculated using the spin-polarized transmission function presented in Fig. 1a. Let us discuss first the electrical conductance. The corresponding results obtained for the spin-up, $G_\uparrow$, and spin-down, $G_\downarrow$, channels are presented in Fig. 3. The

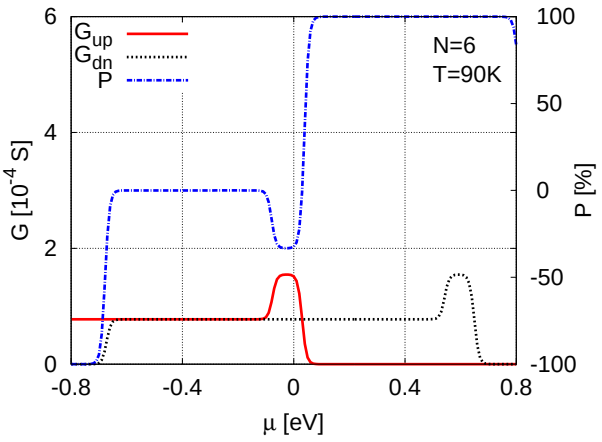

Fig. 3 (Color online) Spin-resolved electrical conductance of the 2HB-1HN zBNNRs with $N = 6$ zigzag atomic chains, shown as a function of the chemical potential and calculated for T=90K. Spin polarization P is also shown.

polarization factor P, defined as $P = (G_\downarrow - G_\uparrow)/(G_\downarrow + G_\uparrow) \times 100\%$, is also presented there. It is interesting that the conductance in both spin channels is practically the same in a wide region of chemical potential below the Fermi level E_F, while one spin channel becomes inactive in transport just above E_F. Therefore, the spin polarization factor P can achieve 100 % in a wide region of chemical potential above the Fermi level, and the system can then work as a very efficient spin filter. Importantly, the filtering properties can be easily controlled by a gate voltage applied to the system, which allows to change the chemical potential.

Thermal conductance due to electrons is presented in Fig. 4 as a function of the chemical potential. Since only one spin channel is active in transport for chemical potentials above the Fermi level, the total transmission is diminished and the thermal conductance is also remarkably reduced. This is an important feature from the point of view of thermoelectric properties, because the heat transport is reduced in the same energy region, where the charge transport is quite significant. When

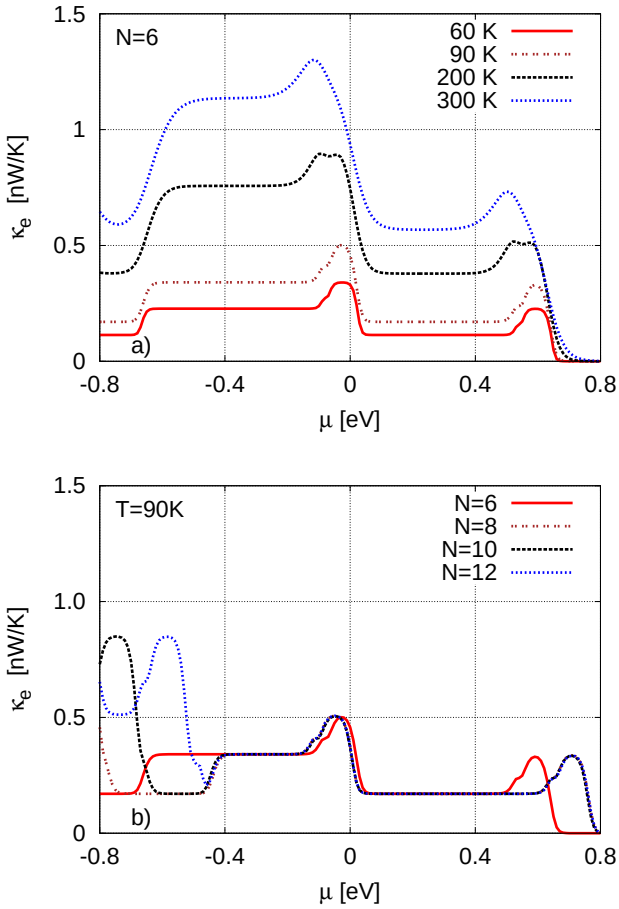

Fig. 4 (Color online) Thermal conductance of 2HB-1HN nanoribbons as a function of the chemical potential for (a) indicated temperatures and $N = 6$ zigzag atomic chains, and (b) for indicated values of the nanoribbon width and $T = 90$ K.

the temperature increases, the thermal conductance is considerably enhanced in a wide energy region below the Fermi energy E_F. However, the appropriate enhancement above the Fermi energy is not well pronounced, so the thermal conductance in this region remains relatively low, even at room temperature, see Fig. 4a. Dependence of the heat conductance on the nanoribbon width is shown in Fig. 4b. Note, in a broad region of chemical potentials the heat conductance is almost independent of the nanoribbon width. Remarkable differences appear for $|\mu| > 0.4$ eV.

Let us investigate now the conventional (charge) S_c and spin S_s Seebeck coefficients. The corresponding numerical results are shown in Fig. 5, where both S_c and S_s are presented as a function of the chemical potential. Due to the fact that the transmission $T_\sigma(E)$ in each spin channel is constant in wide

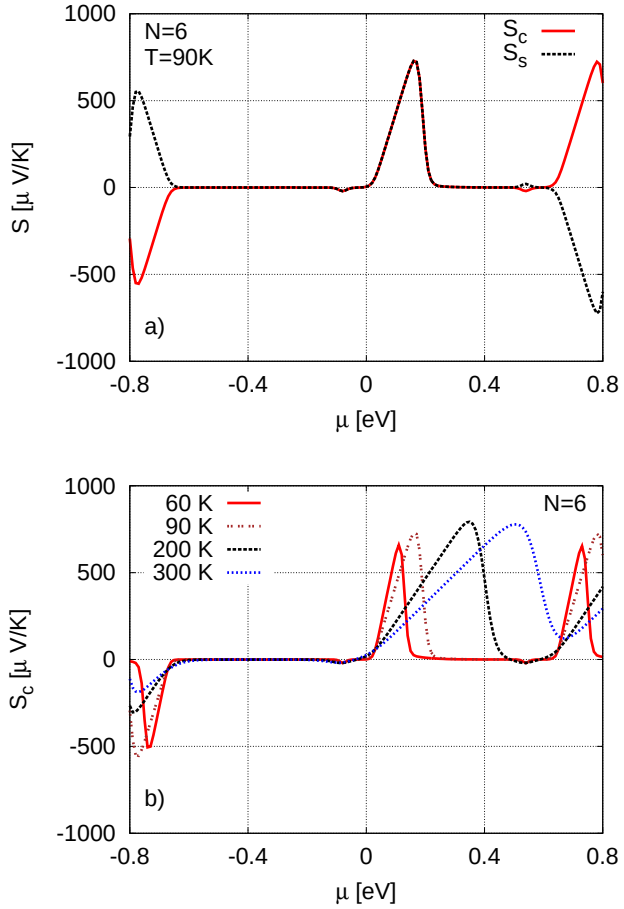

Fig. 5 (Color online) (a) Conventional S_c and spin S_s thermoelectric coefficients for the 2HB-1HN zBNNRs as a function of chemical potential, calculated for $N = 6$ and $T = 90$ K. (b) The coefficient S_c for $N = 6$ and indicated values of temperature.

energy regions below and above the Fermi level, there is practically no contribution to the Seebeck coefficients in these regions. This is because currents due to particles and holes cancel then each other. This also follows from the Mott's relation, according to which $S \sim \partial \ln G(\varepsilon)/\partial\varepsilon$ for ε taken at the Fermi level. Thus, when the transmission is constant, the conductance is constant as well and therefore S vanishes. However, a very high peak appears in the vicinity of E_F as a result of rapid decrease of transmission with increasing energy E in the spin-up channel, which becomes non-conductive above E_F. Then, the contributions due to particles and holes do not cancel each other. On the contrary, the transmission function in the spin-down channel remains constant, so this channel does not contribute to the Seebeck coefficients. In such a situation both S_c and S_s are practically equal. A different behavior can be observed for chemical potentials far below and far above the Fermi energy, where S_c and S_s have opposite signs (see Fig. 5a), which indicates that only the spin-down channel contributes to both Seebeck coefficients in this particular situation. Variation of the conventional Seebeck coefficient with temperature is presented in Fig. 5b. One can note, that the main peak in S_c is shifted with increasing T towards higher values of the chemical potential. Moreover, due to a broadening of the Fermi-Dirac distribution function, the peak becomes then wider and slightly higher.

The presented results clearly show that the nanoribbons of type 2HB-1HN, considered in this section, can exhibit very high conventional and spin Seebeck effects for chemical potentials in a close vicinity of the Fermi energy E_F – even if they have metallic transport properties. This results from the very specific band structure of these nanoribbons. It is also interesting to note, that this asymmetrically hydrogenated system exhibits some features which are similar to the corresponding features of the nanoribbons with both bare edges, especially for energies close to and above the Fermi energy E_F. In both systems the spin-up transmission rapidly decreases above E_F, and this spin channel becomes non-conductive for higher energies, while the second spin channel is then fully active in transport. Quite different behavior can be observed in nanoribbons of 2HB-2HN and 1HB-2HN types, where both spin channels appear to be conductive practically in the same energy regions, as one can conclude from Fig. 1.

5 Thermoelectric efficiency of zBNNRs

Thermoelectric efficiency of a system is described by the figure of merit, defined as

$$ZT_c = \frac{S_c^2 (G_\uparrow + G_\downarrow) T}{\kappa_e + \kappa_{ph}}, \tag{3}$$

where $G = G_\uparrow + G_\downarrow$ is the total electrical conductance, while κ_{ph} denotes here the heat conductance due to phonons. Similarly, one can introduce the spin thermoelectric efficiency by the formula

$$ZT_s = \frac{S_s^2 |G_\uparrow - G_\downarrow| T}{\kappa_e + \kappa_{ph}}, \tag{4}$$

where $G_\uparrow - G_\downarrow$ corresponds here to the spin conductance.

The spin thermoelectric efficiency calculated for the four systems under consideration is presented in Fig. 6a. The phonon heat conductance for the nanoribbons was estimated on the basis of Ref.[45], and following this paper we assumed κ_{ph}=0.3 nW/K at 90K for $N = 6$. It appears that the conventional ZT_c and spin ZT_s figures of merit exhibit very similar behavior, so we focus mainly on the results for the spin one. Very interesting results have been obtained for the nanoribbons of 2HB-1HN type, where ZT_s has two high peaks; the one

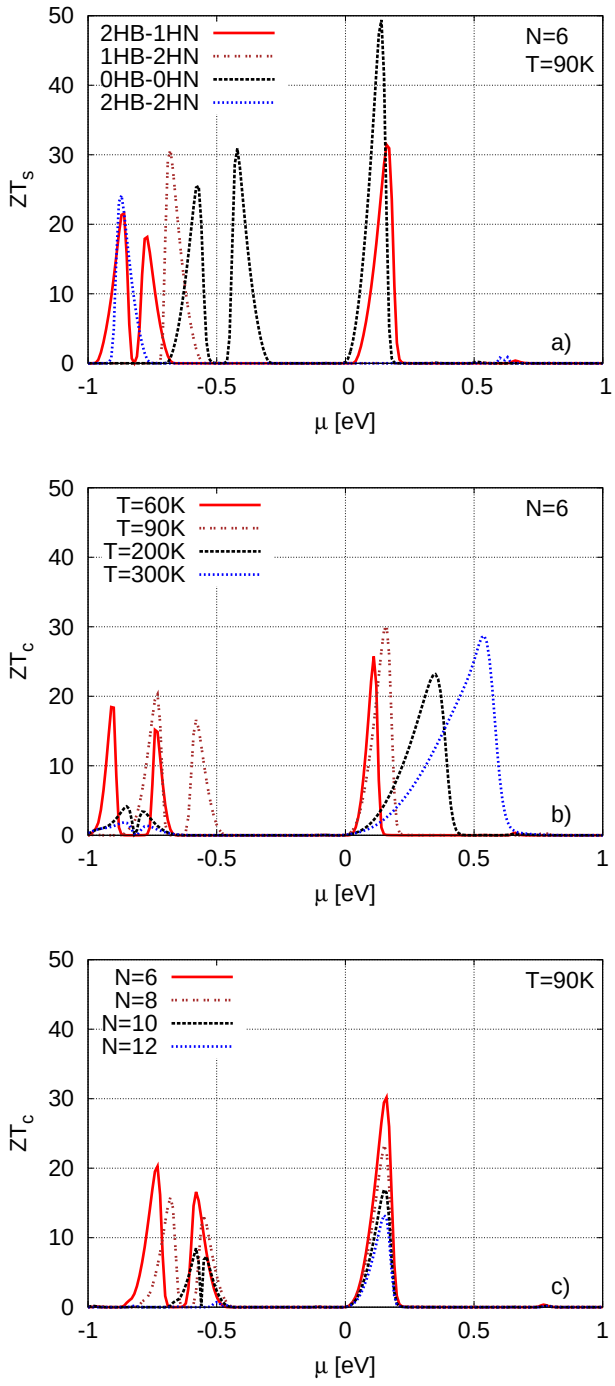

Fig. 6 (Color online) (a) Spin thermoelectric efficiency ZT_s of the zBNNRs of indicated types as a function of the chemical potential for $T = 90$ K, $N = 6$ atomic chains. (b) Conventional thermoelectric efficiency ZT_c of the 2HB-1HN zBNNRs, calculated for indicated temperatures and N. (c) Conventional thermoelectric efficiency of the 2HB-1HN zBNNRs for indicated nanoribbon widths and T=90K. κ_{ph} for different temperatures and nanoribbons widths taken from Ref[45].

(higher) just above the Fermi level and the second (considerably lower) for chemical potentials far below E_F. The higher peak results from the rapid decrease in the spin-up transmission, when this channel becomes non-conductive and leads to the high peak in the Seebeck coefficient. It is important that the second spin channel is still fully conductive in this energy region, so the electrical conductance remains constant and thus enhances the thermoelectric efficiency. Its influence on ZT_s and ZT_c can be very well seen for nanoribbons with bare edges. In this system the transmission of the spin-down channel is very high above the Fermi level, which leads to considerably high spin and charge conductance and, as a result, pronounced peaks appear in ZT_s and ZT_c just above E_F. Moreover, the two peaks for μ below E_F, which appear in ZT_s and ZT_c, are closer to the Fermi energy E_F in nanoribbons with bare edges than in nanoribbons of the 2HB-1HN type. These peaks come from the edges of wide energy gap in the spin-up channel, which is present in the transmission for chemical potentials lower than E_F. The obtained results clearly show that the nanoribbons of 2HB-1HN type, and especially the ones with bare edges, 0HB-0HN, are very promising systems for conversion of thermal energy into the electric one in nanoelectronic and spintronic devices. This appears due to exceptional electronic and thermoelectric properties of these nanoribbons.

Temperature variation of ZT_s and ZT_c is very important from the point of view of potential applications, as the thermoelectric efficiency of a good thermoelectric material should be high enough at room temperature. According to Fig. 6b, a high conventional thermoelectric efficiency in 2HB-1HN zBNNRs can be expected even at room temperature. A slight increase of ZT_c at room temperature can be ascribed to the fact that the main maximum in S_c is shifted at high temperatures to the region where the thermal conductance due to electrons is reduced when the gap becomes open in the spin-down channel (see Figs 1 and 4). According to Fig. 6c, height of the main peak in ZT_c becomes reduced with increasing nanoribbon width, but remains relatively high up to N=12.

On the other hand, properties of the nanoribbons of 2HB-2HN and 1HB-2HN types are much less pronounced. Constant transmission in a wide energy region in the 2HB-2HN system leads to rather small values of ZT_s and ZT_c, apart from the peaks which appear for large negative values of the chemical potential. Similarly, a high peak also appears in the asymmetrically terminated 1HB-2HN nanoribbons, which however is relatively far from the Fermi level.

We have also calculated the band structure and transport properties of the zBNNRs with both mono-hydrogenated edges and of the zBNNRs with one edge bare and the other one mono-hydrogenated. Two of them, i.e. 0HB-1HN and 1HB-1HN nanoribbons have semiconductor properties, but with very wide energy gaps which make the experimental observation of the thermoelectric properties rather impossible, espe-

cially at low temperatures. The other systems, i.e. 1HB-0HN and 0HB-2HN nanoribbons, are metallic and exhibit relatively high thermoelectric efficiency ZT_c close to 25 and $ZT_s \approx 8$, but the peaks appear rather far below the Fermi Energy E_F. Moreover, these structures are less stable.

All the results presented above show very clearly that hydrogenation of zBNNRs has a very huge impact on the transport and thermoelectric properties of these systems. Thermoelectric efficiency can be very low (2HB-2HN systems) or significantly enhanced (0HB-0HN, 2HB-1HN) in dependence on the degree of the edge hydrogenation.

6 Summary and conclusions

Electric and thermoelectric transport properties of hydrogen terminated boron nitride nanoribbons of zigzag type have been analyzed theoretically. From the electronic band structure determined by the *ab-initio* method based on the DFT formalism, we have calculated electric and thermal conductance as a function of the chemical potential, as well as the corresponding thermoelectric coefficients. The numerical results clearly show that the edge hydrogenation strongly influences electric and thermoelectric properties of the nanoribbons. In dependence on the number of hydrogen atoms attached to B or N edge atoms, the systems can reveal either wide-gap semiconducting or metallic transport features, and thus can exhibit very different thermoelectric properties.

The nanoribbons of 2HB-1HN and 0HB-0HN types appear to be ideal thermoelectric materials, with a great potential for applications in nanoelectronic and spintronic devices. These nanonribbons exhibit high thermoelectric efficiency, both conventional and spin ones, described by the appropriate figures of merit ZT_c and ZT_s, respectively. This exceptional thermoelectric efficiency results from the very peculiar band structure of these nanoribbons, with one spin channel inactive in transport just above the Fermi energy E_F of the corresponding charge neutral systems. Accordingly, in the presence of an appropriate gate voltage, which enables controlling position of the corresponding Fermi level, the systems can become half-metallic. Moreover, the transmission of the conducting channel is relatively high and flat in this energy region, leading thus to a considerable electrical conductance. The conducting channel does not contribute to the Seebeck coefficients, but a rapid decrease of transmission just above the Fermi energy E_F in the spin-up channel results in a strong enhancement of both S_c and S_s.

Finally, the total thermal conductance due to electrons and due to phonons is relatively small. It appears that κ_{ph} at low temperatures is much lower than the phonon conductance in other one-dimensional systems, like silicene or grapheme nanoribbons. Accordingly, zigzag boron nitride nanoribbons of 2HB-1HN and 0HB-0HN types exhibit all three features responsible for high thermoelectric efficiency: 1) half-metallicity, 2) rapid decrease of one-spin channel transmission near the Fermi energy E_F, and 3) low phonon conductance. Therefore, these systems seem to be ideal ones for conversion of heat into electrical energy at nanoscale.

7 Acknowledgments

This work was supported by the National Science Center in Poland as the Project No. DEC-2012/04/A/ST3/00372. Numerical calculations were performed at the Interdisciplinary Centre for Mathematical and Computational Modelling (ICM) at Warsaw University and supported in part by PL-Grid Infrastructure.

References

1 D. Pacile, J. C. Meyer, C. O. Girit, and A. Zettl, Appl. Phys. Lett. **92**, 133107 (2008).
2 W-Q. Han, L. Wu, Y. Zhu, K. Watanabe, and T. Taniguchi, Appl. Phys. Lett. **93**, 223103 (2008).
3 M. Corso, T. Greber, and J. Osterwalder, Surf. Sci. **577**, L78 (2005).
4 C. Zhi, Y. Bando, C. Tang, and D. Golberg, Mater. Sci. Eng, R **70**, 92 (2010)
5 C. Zhi, Y. Bando, C. Tang, H. Kuwahara, and D. Golberg, Adv. Mater. **21**, 2889 (2009).
6 C. Zhi, Y. Bando, C. Tang, Q. Huang, and D. Golberg, J. Mater. Chem. **18**, 3900 (2008).
7 N. G. Chopra, R. J. Luyken, K. Cherrey, V. H. Crespi, M. L. Cohen, S. G. Louie, and A. Zettl, Science **269**, 955 (1995).
8 A. Nag, K. Raidongia, K. P. S. S. Hembram, R. Datta, U. V. Waghmare, and C. N. R. Rao, ACS Nano **4**, 1539 ((2010).
9 Y. Shi, C. Hamsen, X. Jia, K. K. Kim, A. Reina, M. Hofmann, A. L. Hsu, K. Zhang, H. Li, Z.-Y. Juang et al., Nano Lett. **10**, 4134 (2010).
10 Y. Lin, T. V. Williams, W. Cao, H. E. Elasyed-Ali, and J. W. Connell, J. Phys. Chem. C **114**, 17434 (2010).
11 L. Ci, L. Song, C. Jin, D. Jariwala, D. Wu, Y. Li, A. Srivastava, Z. F. Wang, K. Storr, L. Balicas, et al., Nat. Mater. **9**, 430 (2010).
12 L. Song, L. Ci, H. Lu, P. B. Sorokin, C. Jin, J. Ni, A. G. Kvashnin, D. G. Kvashnin, J. Lou, B. I. Yakobson, et al., Nano Lett. **10**, 3209 (2010).
13 C. Li, Y. Bando, C. Zhi, Y. Huang, and D. Golberg, Nanotechnology **20**, 385707 (2009).
14 H. Zeng, C. Zhi, Z. Zhang, X. Wei, X. Wang, W. Guo, Y. Bando, and D.Golberg, Nano Lett. **10**, 5049 (2010).

15 M. Topskal, E. Akturk, and S. Ciraci, Phys. Rev. B **79**, 115442 (2009).
16 F. Zheng, G. Zhou, Z. Liu, J. Wu, W. Duan, B.-L. Gu, and S. B. Zhang, Phys. Rev. B **78**, 205415 (2008).
17 L. Lai, J. Lu, L. Wang, G. Luo, J. Zhou, R. Qin, Z. Gao, and W. Mei, J. Phys. Chem. C **113**, 2273 (2008).
18 F.-L. Zheng, Y. Zhang, J.-M. Zhang, and K.-W. Xu, J. Phys. Chem. Sol. **72**, 256 (2011).
19 C. H. Park, and S. G. Louie, Nano Lett. **8**, 2200 (2008).
20 Y. Wang, Y. Ding, and J. Ni, Phys. Rev. B **81**, 193407 (2010).
21 J. Qi, X. Qian, L. Qi, J. Feng, D. Shi, and J. Li, Nano Lett. **12**, 1224 (2012).
22 H. Wan, B. Zhou, W. Liao, and G. Zhou, J. Chem. Phys. **138**, 034705 (2013).
23 C. Sevik, A. Kinaci, J. B. Haskins, and T. Cagin, Phys. Rev. B **84**, 085409 (2011).
24 F. Mazzamuto, V. Huang Nguyen, Y. Apertet, C. Caer, C. Chassat, J. Saint-Martin and P. Dollfus, Phys. Rev. B **83**, 235426 (2011).
25 Y. Ding and J. Ni, Appl. Phys. Lett. **95**, 083115 (2009); W. Zhao, Z. X. Guo, J. X. Cao, and J. W. Ding, AIP Advances **1**, 042135 (2011).
26 T. G. Pedersen, C. Flindt, J. Pedersen, N. A. Mortensen, A. P. Jauho, and K. Pedersen, Phys. Rev. Letters **100**, 136804 (2008).
27 Y. Yan, Q. F. Liang, H. Zhao, C. Q. Wu, and B. Li, Phys. Letters A **376**, 2425 (2012).
28 X. Ni, G. Liang, J.-S. Wang, and B. Li, Appl. Phys. Lett. **95**, 192114 (2009).
29 M. Wierzbicki, R. Swirkowicz, and J. Barnaś, Phys. Rev. **88**, 235434 (2013).
30 K. Zberecki, M. Wierzbicki, J. Barnaś, and R. Swirkowicz, Phys. Rev B **88**, 115404 (2013).
31 L. Pan, H. J. Liu, X. J. Tan, H. Y. Lv, J. Shi, X. F. Tang, G. Zheng, Phys. Chem. Chem. Phys. **14**, 13588 (2012).
32 K. Yang, Y. Chen, R. D'Agosta, Y. Xie, J. Zhong, and A. Rubio, Phys. Rev. B **86**, 045425 (2012).
33 M. Walter, J. Walowski, V. Zbarsky, M. Münzenberg, M. Schäfers, D. Ebke, G. Reiss, A. Thomas, P. Peretzki, M. Seibt, J.S. Moodera, M. Czerner, M. Bachmann, Ch. Heiliger, Nature Mat. **10**, 742 (2011).
34 N. Liebing, S. Serrano-Guisan, K. Rott, G. Reiss, J. Langer, B. Ocker, and H. W. Schumacher, Phys. Rev. Lett. **107**, 177201 (2011).
35 K. Uchida, S. Takahashi, K. Harii, J. Ieda, W. Koshibae, K. Ando, S. Maekawa, E. Saitoh, Nature **455**, 778 (2008).
36 M. Wierzbicki, R. Swirkowicz, and J. Barnaś, Phys. Rev. B **80**, 195409 (2009).
37 Y.-W. Son, M. L. Cohen, S. G. Louie, Phys. Rev. Lett. **97**, 216803 (2006).
38 K. Uchida, H. Adachi, T. An, T. Ota, M. Toda, B. Hillebrands, S. Maekawa, and E. Saitoh, Nature Mater. **10**, 737 (2011).
39 S. Y. Huang, W. G. Wang, S. F. Lee, J. Kwo, and C. L. Chien, Phys. Rev. Lett. **107**, 216604 (2011).
40 J. C. Le Breton, S. Sharma, H. Saito, S. Yuasa, and R. Jansen, Nature **475**, 82 (2011).
41 J.P. Perdew, K. Burke, and M. Ernzerhof. Phys. Rev. Lett., 77, 3865 (1996).
42 Ch. Lee, W. Yang and R. G. Parr, Phys. Rev. B 37 (2): 785789 (1988).
43 D. Sanchez-Portal, P. Ordejon, E. Artacho, J. M. Soler,Int. J. Quantum Chem. 65, 453 (1997).
44 M. Brandbyge, J.-L. Mozos, P. Ordejon, J. Taylor, K. Stokbro, Phys. Rev. B 65, 165401 (2002).
45 T. Ouyang, Y. Chen, Y. Xie, K. Yang, Z. Bao and J. Zhong, Nanotech. **21**, 245701 (2010).